GPS Antenna Characterization Experiment (ACE): Receiver Design and Initial Results

Philip D. Martzen, Dolan E. Highsmith, *The Aerospace Corporation*
Jennifer E. Valdez, Joel J. K. Parker, Michael C. Moreau, *Goddard Space Flight Center, NASA*

Abstract

The GPS Antenna Characterization Experiment (ACE) is a research collaboration between Aerospace and NASA Goddard to characterize the gain patterns of the GPS L1 transmit antennas. High altitude GPS observations are collected at a ground station through a transponder-based or "bent-pipe" architecture where the GPS L1 RF spectrum is received at a platform in geosynchronous orbit and relayed to the ground for processing. The focus of this paper is the unique receiver algorithm design and implementation. The high-sensitivity GPS C/A-code receiver uses high fidelity code and carrier estimates and externally supplied GPS message bit data in a batch algorithm with settings for a 0 dB-Hz threshold. The resulting carrier-to-noise measurements are used in a GPS L1 transmit antenna pattern reconstruction. This paper shows initial transmit gain patterns averaged over each block of GPS satellites, including comparisons to available pre-flight gain measurements from the GPS vehicle contractors. These results provide never-before-seen assessments of the full, in-flight transmit gain patterns.

1 Introduction

High-altitude space users of GPS rely on the GPS main beam signals that spill over the limb of the earth. These users are, in effect, "squinting" at GPS vehicles that are almost directly on the opposite side of the earth, while a much larger range of signals is available within the GPS side lobes. Figure 1 shows the additional coverage afforded by side lobes out to 60 deg off-boresight from a GPS transmitter. The side lobe signals offer significant potential to increase the accuracy of high-altitude GPS navigation performance through an increased number of GPS satellites available to track and correspondingly greater geometric diversity. However, very little is known about the in-flight performance of the side lobe signals because they cannot be observed from the direct line-of-sight to receivers on the ground. Furthermore, the currently operational blocks of GPS satellites do not have a requirements for received power or signal quality performance in the side lobes, so the GPS vehicles have not had to be tested for a specified performance outside the main beam. The lack of knowledge of side lobe quality and thresholds on orbit adds risk to missions that seek to employ the side lobes to meet navigation requirements.

The GPS Antenna Characterization Experiment (ACE) seeks to fill that knowledge gap through a collaboration between The Aerospace Corporation and NASA Goddard Space Flight Center to collect and analyze observations from GPS side lobe transmissions to a satellite in geosynchronous orbit (GEO) using highly-sensitive GPS receivers installed at a ground station. This is enabled by the existence of a "bent-pipe" architecture whereby the GEO vehicle collects the GPS L1 RF spectrum and relays it to a ground station for processing, similar to the architecture described by Kronman in Ref. [1]. For GPS signal in space (SIS) and Space Service Volume (SSV) characterization, the availability of the full set of GPS signals at the ground station represents a unique opportunity for thorough analysis of in-flight performance of side lobe signals of the entire constellation over a long period of time. This data set is unique and offers many opportunities for varied analyses to improve our understanding of different aspects of the system, such as signal power and pseudorange accuracy as a function of off-boresight angle, as well as verification of performance assumptions made in GPS simulations. The end results enable more effective and more accurate use of GPS for navigation of high-altitude satellites. This paper focuses on the unique receiver algorithm design and

implementation of one of the receivers deployed as part of the experiment, along with reconstructed GPS L1 transmit gain patterns.

2 Previous Work to Characterize Signals in Space

High altitude GPS performance has been of great interest to the GPS community since the 1990s. Early works of note on GPS receiver architectures for High Earth Orbit (HEO) navigation include Moreau's thesis on receiver algorithms for autonomous on-board navigation [2] and Kronman's paper describing the bent-pipe system used to navigate a GEO satellite from a ground station [1]. Because of the dearth of published ground test data and in-flight observations of GPS side lobes, research on GPS usage in HEO has relied on theoretical performance in the side lobes, if not entirely ignoring them in favor of tracking only the main beam spillover around the limb of the earth.

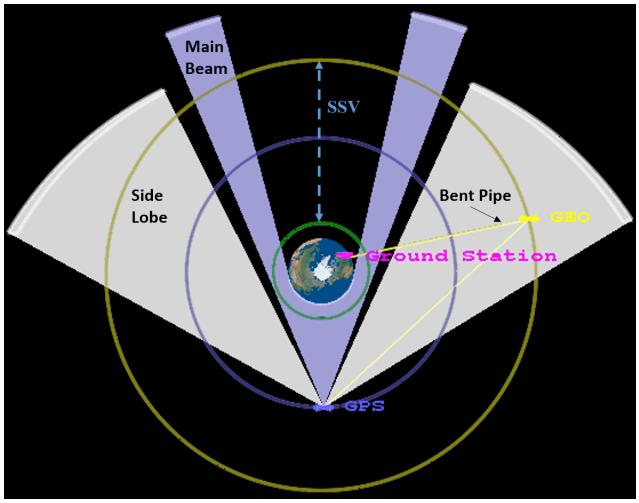

Figure 1: GPS main beam and side lobe coverage out to 60 deg off-nadir. Space Service Volume (SSV) ranges from 3,000 km to 36,000 km altitude. Bent-pipe architecture shows transmissions from GPS to GEO vehicle being relayed to a ground station.

For many years, the only data published on the GPS L-band antenna pattern consisted of four azimuth cuts of the relative gain from the Block II antenna [3]. Early high altitude GPS flight experiments conducted in the late 1990s such as the Air Force Academy mission Falcon Gold in 1997 [4], the ESA Equator-S mission [5], and the NASA Goddard / AMSAT OSCAR-40 mission in 2000 [6] provided a very limited amount of data on actual GPS signal levels. Nevertheless, there were enough data, particularly from the AMSAT OSCAR-40 experiment, to make it clear that significant variations existed in the transmitted power levels, not just within the side lobes, but also within the main lobe signals beyond the Earths limb. These differences were subsequently confirmed through the extensive ground measurements performed by Lockheed Martin of the Block IIR and IIR-M antenna panels prior to launch; however, these data were not available to the general user community.

To address this lack of consistency in the signal power levels for HEO users, Bauer et al. proposed metrics for GPS signal performance requirements in two SSV regimes: medium altitudes from 3,000 km to 8,000 km and high/geosynchronous altitudes from 8,000 km to 36,000 km [7]. A key missing piece, however, is knowledge of the actual on-orbit signal performance for comparison to proposed requirements on future blocks, to validate theoretical models, and to enable usage of the side lobes of current vehicles with confidence.

More recently, better information has become available on the actual transmitted GPS signals. The European Space Agency published GIOVE-A GPS receiver results in 2013 with gain measurements from each GPS block averaged over azimuth and extending to 58 deg off-boresight with IIR vehicles, but only to 37 deg off-boresight with IIF vehicles [8]. While the GIOVE-A results are the most extensive to date, they lack resolution in azimuth and into the far side lobes due to operational constraints and an orbit that is only slightly above the GPS constellation. Furthermore, Lockheed Martin has recently made publicly available its measurements of L-band transmit gain patterns for each Block IIR and IIR-M antenna panel [9]. These data sets provide the most extensive look at full broadcast gain patterns with resolutions as fine as 1 deg by 1 deg out to 90 deg off-boresight and 360 deg in azimuth. While very useful for simulations of the current constellation, there is still limited to no data available on the Block II/IIA/IIF satellites built by Boeing, and questions remain as to how representative these patterns are on orbit and over the long lifetimes of the GPS vehicles, as well as the nature of the error characteristics of the side lobe signals. The extensive data set collected by GPS ACE addresses many of the unknowns in the on-orbit performance of the GPS signal in space.

3 GPS ACE Project Description

Aerospace and NASA Goddard began the GPS ACE project through respective independent research and development efforts in FY2013, with collaboration authorized through a NASA Space Act Agreement. The project began with significant receiver development efforts on both sides. Aerospace produced the Mariposa GPS Receiver (MGPSR), a heavily aided, extremely weak signal tracking software receiver described in Section 4. NASA contributed two versions of its Navigator GPS Receiver platform [10]: one implemented completely in software, as well as an FPGA-based implementation. The receiver technologies are complementary; the MGPSR represents an advanced receiver for implementation in a non-real-time navigation ground architecture, while the Navigator implements an on-board, unaided algorithm for weak-signal tracking and autonomous navigation in real time at high altitudes.

The next step involved installing the receiver hardware into an existing bent-pipe architecture for a GEO platform. The resulting GPS ACE data collection architecture is depicted in Figure 2.

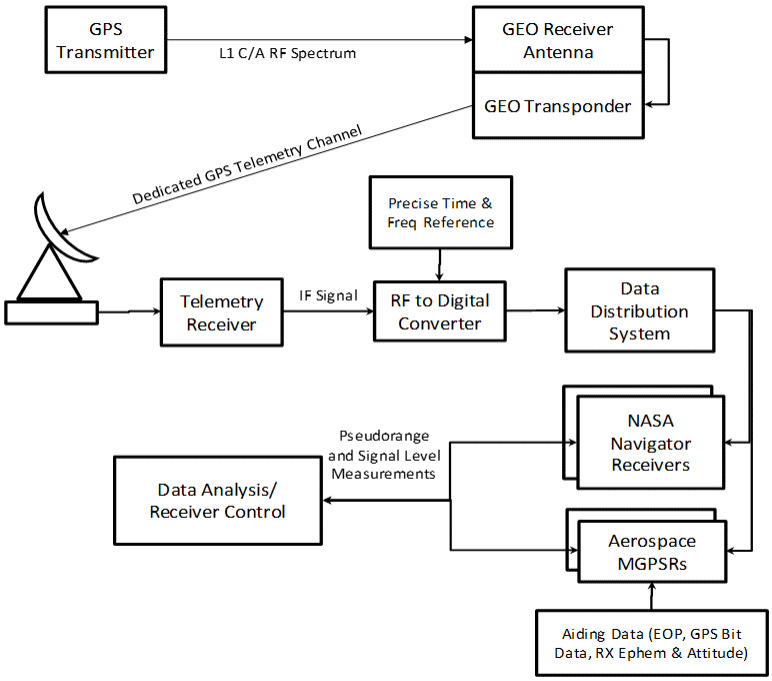

Figure 2: GPS ACE data collection architecture.

Beginning at the top left in Figure 2, the GPS vehicles transmit L1 C/A at 1575.42 MHz to a GEO platform with a patch antenna. A sample bandwidth centered around L1 is downconverted using a ground-based reference and transponded to the ground station on a dedicated telemetry channel, such that the GPS L1 spectrum is continuously available at the station. The downconverted intermediate frequency (IF) is digitized into packets. The autonomous GPS receivers pull the packetized data from the local network, process the data and output GPS observation files containing pseudorange, carrier and carrier-to-noise ratio measurements. Multiples of each receiver type are installed to permit flexibility and redundancy. Network access allows for data analysis and receiver monitoring from outside the ground station.

The hardware was installed at the ground station in early 2014, at which point the NASA Navigator receivers began recording observation data. The Aerospace MGPSRs required additional configuration and tuning such that they began producing the desired data quality in May 2014. Given the continuous availability of the GPS L1 spectrum at the ground station, the GPS ACE receivers produce daily observation files with a full 24 hours of tracking down

to the sensitivity of the respective receivers: 22 dB-Hz for the NASA Navigator at 20 msec integrations and less than 0 dB-Hz for the Aerospace MGPSR at 30 sec integrations. The extreme sensitivity of the MGPSR enables reconstruction of the GPS transmit gain patterns deep into the far side lobes. The following sections describe the MGPSR algorithm and how the resulting received signal strength measurements are used to produce maps of the in-flight transmit gain patterns.

4 Mariposa GPS Receiver (MGPSR) Algorithm

The Mariposa GPS Receiver (MGPSR) uses a highly aided, long integration batch processing algorithm. It was developed to operate in a non-real-time ground environment and process low SNR digital samples of GPS RF collected at orbital altitudes. Its roots derive from the data processing of the US Air Force Academy sponsored experiment Falcon Gold that was flown in November 1997 to measure GPS signals at high orbital altitudes [4]. The Falcon Gold data set, collected in a geosynchronous transfer orbit, contributed to the MGPSR design objectives and was recently used in work at the University of Colorado [11].

The current algorithm and design approach derive from orbit determination applications involving weak signal bent-pipe GPS in an aided post-processing mode. In this mode the GPS base-band data is captured and queued for processing a short time later when aiding information is available: a) GPS ephemeris and clock (from subframe data), b) approximate transponder ephemeris, and c) raw GPS subframe bit data from other sources. The subframe bit data effectively enables data wiping and long coherent processing, while good ephemeris and clock enable reduced search. The aiding information is combined to form the parameters of the expected received GPS signal.

The MGPSR, like many GPS receivers, is a hypothesis tester [12]. It forms a hypothesis GPS signal which it then correlates with the actual received signal. If the actual received signal is above the detection threshold, and if the hypothesis matches the actual signal, the hypothesis tester registers an output. More significantly the successful hypothesis parameters represent the desired measurement outputs.

In most receivers, the residual offset errors would be applied to the tracking loop or signal model parameters to refine the hypothesis and to zero out the residual tracking loop error. Then the corrected signal parameters would represent the desired outputs. Instead, the MGPSR operates in a batch or block mode as opposed to a tracking model [13, 14]. Because the MGPSR is normally operated in the small initial residual offset region and because nearly linear discriminators are used, the output error closely approximates the *a priori* pseudorange error. Thus, assuming the output error is a good estimate of the pseudorange error, the error signal is applied to the *a priori* pseudorange to generate the corrected output.

4.1 Signal Model

The MGPSR model for the digitized signal from the intermediate frequency (IF) analog-to-digital (A2D) converter can be described with Figure 3. In general, this signal originates from the GPS satellite, is received by the transponder, is down converted with an ideal mixer using a ground based local oscillator (LO) frequency, then is transmitted to the ground where it is digitized.

The light time diagram in Figure 3 provides a notional graphical solution for the signal propagation time between points in space. The notional range is on the y-axis and time is on the x-axis. The time line of an object lies along a nearly horizontal line (where the slope is the velocity). Light and radio signals travel at the speed of light between the time lines of objects. The light time diagram shows the earlier time of transmission of the signal digitized by the A2D converter at time t_5. This signal is a combination of a GPS signal and a LO signal. The GPS signal was transmitted by the GPS SV at time t_4 and arrived at the transponder at time t_{3a}. The LO signal was transmitted at time t_1 and arrived at the transponder at time t_2. The two signals were combined in the ideal mixer at time t_3 to form the down-converted GPS (IF) signal. This signal left the transponder at time t_{3b} and arrived at the ground at time t_{5a}. After a ground delay it arrives at the A2D converter at time t_5. Suppose the GPS signal transmitted at time t_4 contains the SV PRN code phase time t_{sv}. This signal is digitized into a sample at time t_5. The GPSR effectively detects and reports the transmitted code phase time in the sample, reporting the raw pseudorange t_5 -

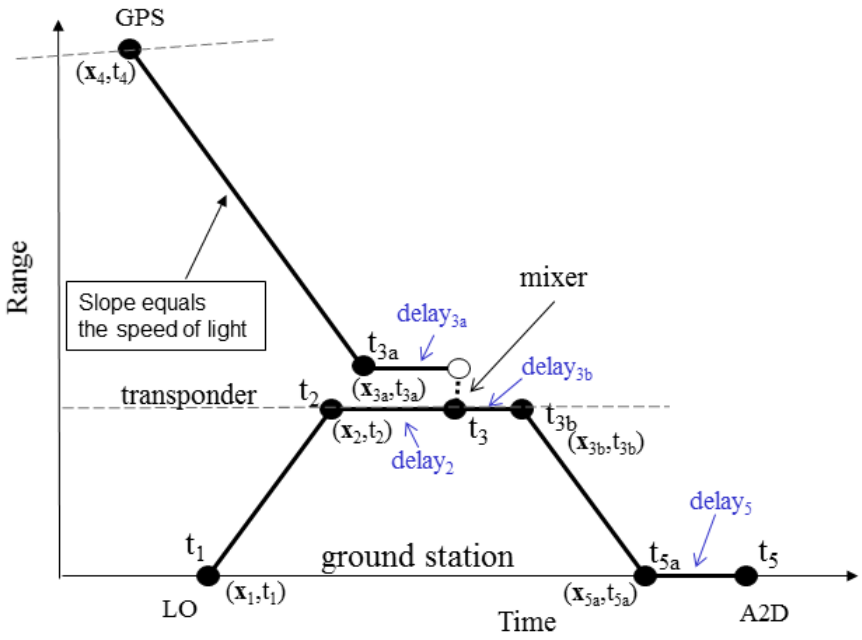

Figure 3: Signal Model Light Time Diagram.

t_{sv}, the sample time minus the code phase time. The carrier phase into the A2D converter at time t_5 is the GPS carrier phase at t_4 minus the LO phase at t_1.

In equation form, the signal model is expressed in terms of the propagation delay "retarded time" [15, p. 185] as

$$t' = t - \frac{\left|\vec{X}(t) - \vec{X}'(t')\right|}{c} \tag{1}$$

where a signal emitted at position $\vec{X}'$ and earlier time t' is received at position $\vec{X}$ and time t. Let the signal captured by the A2D converter at time t_5 be

$$y(t_5) = Ad(t_{sv})ca(t_{sv})e^{j2\pi(f_{GPSL1}t_{sv} - f_{LO}t_1)} + \eta \tag{2}$$

The constant A is the signal amplitude. The function $d(t_{sv})$ represents the subframe data, a 50 bps sequence of +1 and -1 values, evaluated at t_{sv}. The argument t_{sv} is the effective SV PRN code phase time transmitted at time t_4.

The function $ca(t_{sv})$ represents the C/A PRN spreading code value contained in the sample. The received carrier phase is the difference between the GPS transmitted carrier phase $f_{GPSL1}t_{sv}$ and the local oscillator transmitted phase $f_{LO}t_1$. The time t_1 is the LO phase time of transmission. The noise is represented by η.

The equation for $y(t_5)$ does not explicitly contain t_5. The times of transmission, t_4 and t_1, are related to t_5 via the "retarded time" equation 1. The equation is non-linear and can not be solved in closed form unless there is no motion. Instead, the solutions are tabulated as functions of t_5 and then converted to polynomials for use in replica signal generation.

The output of the A2D converter is a sequence of samples of $y(t_5)$. We denote this sample sequence by y_k, where $k = 0, 1, 2, ..., n$. If needed we will denote the time of the y_k sample by t_k.

4.2 Long Coherent Integration Method

The objective of the MGSPR is determine the model parameter errors based on the signal samples. This then allows the determination of the raw pseuodrange, $pr = t_5 - t_{sv}$. The model error is found by searching for adjustments which maximize the correlation between the received signal and a signal replica.

Let the signal replica be represented as

$$r(t_5) = d(\hat{t}_{sv})ca(\hat{t}_{sv})e^{j2\pi(f_{GPSL1}\hat{t}_4 - f_{LO}\hat{t}_1)} \tag{3}$$

Where $\hat{t}_{sv}$, $\hat{t}_4$ and $\hat{t}_1$ are the transmitted code phase time and times of transmission predicted from the model. Here the transmit time, $\hat{t}_4$, is used for the GPS carrier phase.

The MGPSR generates a sequence of replica samples corresponding to the A2D converter samples. We denote this replica sample sequence by r_k, where $k = 0, 1, 2, ..., n$.

In this application, the received signal and the replica have a differential delay and differential frequency offset. The objective of the correlation process is to estimate the SNR of received signal and the differential time delay, τ, between the signal and the replica. Long correlations are required to obtain accurate estimates of these parameters at low SNR values. The problem is compounded by the frequency difference between the received signal and the replica. As explained in Ref. [16] it is required to jointly estimate the time delay and the frequency difference in order to obtain either adequately. This is accomplished by computing the complex ambiguity function (CAF)

$$CAF(\tau, \delta f) = \sum_{k=0}^{n} y_k r_{k+i}^* e^{-j2\pi\delta f \Delta t k} \tag{4}$$

In this expression $i = \tau/\Delta t$ is the shift between the signal and replica sample index, and where Δt is the sample rate. The frequency offset is δf. The time offset and the frequency offset parameters are to be searched simultaneously for the $|CAF(\tau, \delta f)|$ peak. If a signal is present, a CAF correlation peak will be found at some delay τ and Doppler δf offset. Then to first order the measured raw pseudorange is $PR_{raw} = t_5 - (t_{sv} + \tau)$. Here t_5 is the time of a representative sample within the correlation interval, and t_{sv} is the corresponding modeled *a priori* SV PRN code phase time.

The MGPSR correlator performs long coherent integration by coherently combining fast Fourier transform (FFT) generated 1-msec complex correlations using methods similar to those described in references [13, 14]. For example, for 30-sec coherent processing, a set of 30,000 1-msec complex correlations are computed and stored. This 2-D array of 1-msec complex correlations is called a pre-CAF (PCAF). Some sub-set of the 1-msec correlation output is stored in each row of the PCAF depending on how well the time offset is known. The PCAF is computed with $\delta f = 0$.

The PCAF rows are coherently combined, rotating by δf to synthesize a frequency offset, forming a long integration $CAF(\tau, \delta f)$ result in the (τ, δf) search space. The objective is to find the τ_p, δf_p corresponding to the largest $|CAF(\tau, \delta f)|$. Once the CAF grid peak is located, an interpolation or refinement is performed to refine the peak location and obtain the output parameters. The method is effective when the frequency offset is much less than 1 kHz. At frequency offsets of 250 Hz or more, there is significant power loss.

This long coherent integration is now discussed in more detail. The processing is divided into baseband collection, ephemeris and clock data preparation, visibility and link analysis, replica description, replica signal generation, PCAF correlation, CAF generation and coarse search, frequency refine, time refine, and phase measurement steps.

4.3 Baseband Collection

Baseband samples from the transponder are received and stored in baseband snapshot files of some manageable size, (nominally two minutes). Sample time-tag information is included at some regular interval with the baseband snapshots. At the completion of each snapshot, a time-tag polynomial is constructed from the time-tags.

4.4 Ephemeris and Clock Preparation

This step involves the assembly of GPS ephemeris and clock and transponder ephemeris over the time span of interest. The ephemeris files are prepared in the Aerospace TRACE [17] binary format in the J2000 reference frame. A GPS PRN correspondence table including GPS SVN, block, antenna panel and PRN is built. A table of GPS T_{gd} values is built from broadcast Subframe 1 data. If applicable attitude information for the transponder GPS receive antenna is also collected.

4.5 Visibility and Link Analysis

The purpose of the MGPSR Visibility and Link Analysis is to determine GPS in view, and to rank processing from expected strongest to weakest signals. This ranking may be used, if desired, in the processing steps below.

4.6 MGPSR Signal Replica Description Construction

A Signal Replica Description is used to encapsulate the signal parameters of the signal model. A GPS signal replica description is built for each candidate GPS PRN correlation interval. The replica description identifies a baseband snapshot file, specifies the snapshot start sample number and time, contains the signal event and sample time polynomials, and contains GPS Subframe bit data in hex format over the correlation time-span. The signal event polynomials are constructed by a) building tabulations of event times using the signal model and the ephemerides, and b) by fitting polynomials to the tabulations. The polynomials are valid over the snapshot time span (nominally two minutes) plus an overlap interval. The event polynomials are scaled to reduce round off, and have as the independent variable, t_1, expressed as seconds from an integer second near the center of the snapshot.

4.7 Replica Signal Generation

The Replica description is used to configure a signal generator for each MGPSR long integration correlation, with the objective of building replica samples, r_k for each baseband sample y_k corresponding to an A2D converter sample time t_k. The configuration process recasts the t_{sv} and t_4 polynomials in terms of the sample time t_5. The carrier phase at the A2D converter is developed as a polynomial in terms of the sample time.

$$\phi_5(t_5) = 2\pi(f_{GPSL1}t_4 - f_{LO}t_1) \tag{5}$$

This is done via a least squares fit to a tabulation of the phase model. The phase polynomial phase reference is midnight of the current day. The objective is to have the replica signal phase be coherent over the day. This allows the 1-msec correlations to be coherently combined.

The signal generator is able to quickly generate replica samples and is used in PCAF generation (next section). The carrier phase is computed using cosine, sine initialization several times over each 1-msec interval. In between trigonometric angle addition rules are applied to recursively compute sine and cosine values. The code phase t_{sv} time is evaluated a few times over the 1-msec interval, and then updated via increment.

4.8 PCAF generation

The pre-caf (PCAF) is an array of successive 1-msec complex correlation functions spanning the coherent integration interval, computed at $\delta f = 0$. Each row of the PCAF is generated by: a) advance the start sample to the next 1-msec interval, b) invoke the signal generator to generate 1-msec of replica samples, c) generate the 1-msec complex correlation for the interval using FFT methods, and d) append the 1-msec correlation output to the PCAF array. In practice the τ offset is fairly well known, thus a subset of each 1-msec correlation function, a few 10s of microseconds, is stored in each row of the PCAF array.

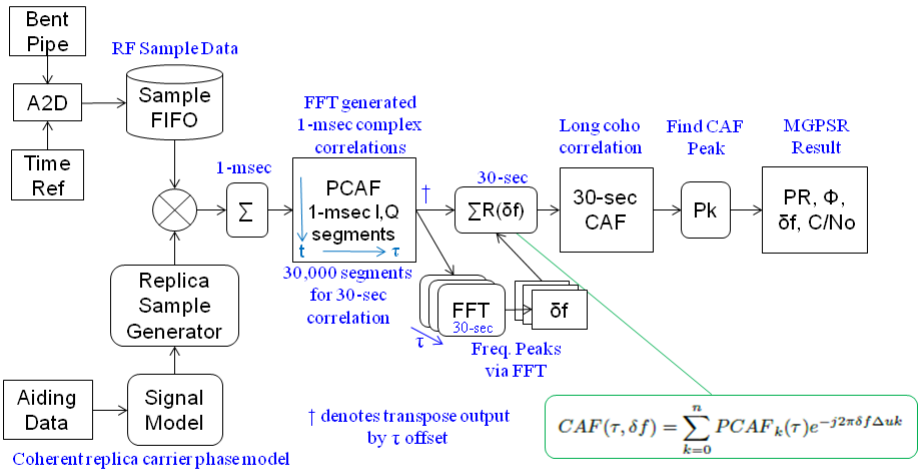

Figure 4: MGPSR Block Diagram

4.9 CAF Generation and Coarse Search

The CAF function is constructed as

$$CAF(\tau,\delta f)=\sum_{k=0}^{n} PCAF_k(\tau)e^{-j2\pi\delta f\Delta uk} \tag{6}$$

Where Δu is the 1-msec PCAF spacing.

The CAF function is normalized to the baseband noise. A detection is declared when the best $|CAF(\tau,\delta f)|$ is 5 or larger [4]. The best value or CAF peak is found by exhaustive search over the τ, δf search space. In the exhaustive search the frequency offset δf is stepped over the search space, evaluating Equation 6 at each τ shift. This process requires some time to execute.

An alternative is to perform an FFT on each column of the PCAF within the τ search region. The FFT quickly generates all the rotations on a grid, generating the CAF surface column much faster. If a signal is present and above the threshold, the FFT output of the peak τ column will have a frequency peak at δf_p.

In summary the procedure is to perform an FFT on each τ column, find the largest FFT output value and record the magnitude and offset. Then if the column best τ magnitude is greater than the τ_{best} magnitude, the τ_{best} and magnitude is updated. This approach is quicker and was adopted as the coarse search method. See Figure 4.

4.10 Fine Frequency

The first step in the fine search process is to interpolate or otherwise refine the frequency peak. *Sinc* function interpolation as a function of frequency on the FFT output of the strongest τ column can be used. This step determines the frequency peak δf_p.

4.11 Fine Time

The next step is evaluate a slice $|CAF(\tau,\delta f_p)|$ of the CAF function for a range of τ values at the best frequency δf_p determined by the fine frequency evaluation. This is done using Equation 6. The fine time is determined by *sinc* interpolation as a function of τ on this slice. This determines the time offset peak τ_p.

4.12 Phase Measurement

The phase measurement is performed on the complex $CAF(\tau, \delta f_p)$ array slice computed in the previous step. Before the phase measurements can be performed, the $CAF(\tau, \delta f_p)$ array must be unwrapped, removing the shift phase offset at non-zero offsets. This phase rotation is present because of the intermediate frequency present in the PCAF. After shift phase unwrap, an $arctan2$ discriminator is applied over the peak samples of the correlation peak to read out the residual phase.

A final rotation is performed on the unwrapped $CAF(\tau, \delta f_p)$ to zero out the Q component, then a $sinc$ interpolation is performed on the I-component to obtain a second τ peak measurement. The second measurement will usually be close to the $|CAF(\tau, \delta f_p)|$ peak measurement, but due to phase distortions is not expected to match exactly. In fact, this may represent an additional means to estimate the measurement error.

4.13 C/N_0 Estimation

The received carrier-to-noise ratio C/N_0 of the received GPS signal is required. This is computed as

$$C/N_0 = 10log_{10}((P-1)/T) \tag{7}$$

where P is the signal to noise power ratio given by $P = \frac{|CAF(\tau,\delta f)|^2}{n\sigma^2}$, and T is the integration time in seconds and σ^2 is the sample variance. When no signal is present, the expected value for P is $P = 1$. These C/N_0 values are the measurements used in reconstructing the GPS transmit antenna patterns.

5 Antenna Pattern Reconstruction

The goal of the antenna pattern reconstruction process is to precisely map individual receiver power measurements and other observed signal characteristics back to the corresponding azimuth and elevation angle of the GPS transmitter, such that GPS signal characteristics may be documented on a per-satellite basis. The MGPSR has produced essentially all-in-view, around-the-clock tracking for over ten months so far. A sample of just one day of MGPSR 30-sec observations from a GEO platform is shown in Figure 5, which illustrates the extent of received signal levels and GPS off-boresight angles available in the data.

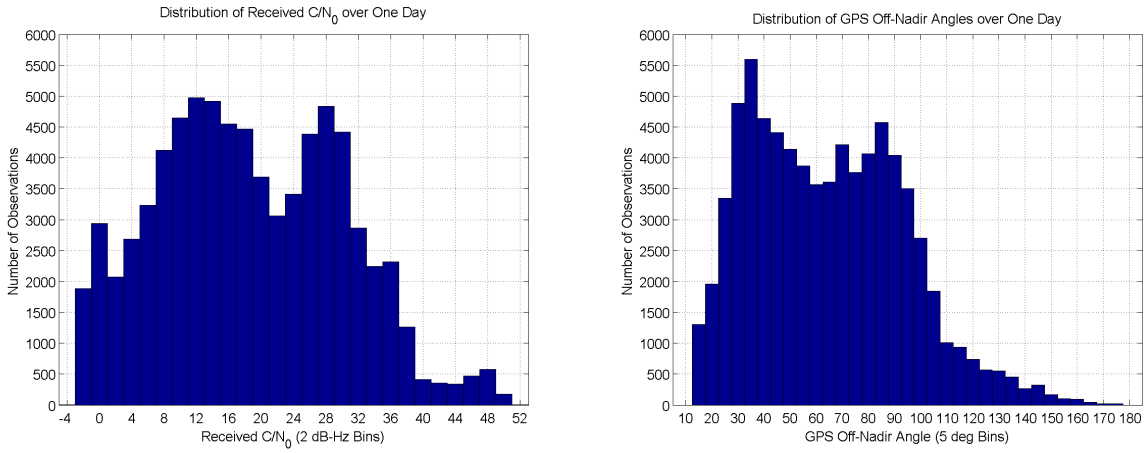

Figure 5: Histograms of the number of MGPSR observations taken over one day from a GEO platform. The left plot shows the distribution of observations with respect to received carrier-to-noise ratio (C/N_0) in 2 dB bins. The right plot shows the distribution with respect to GPS off-nadir or off-boresight angle in 5 deg bins. MGPSR measurements are integrated over a 30-sec interval.

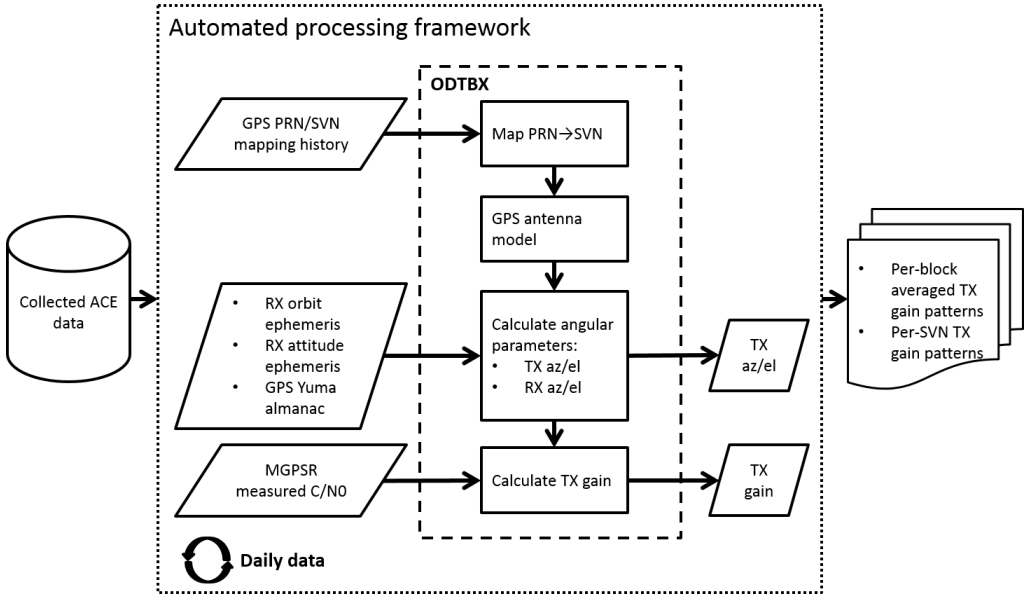

Figure 6: Gain pattern reconstruction process.

5.1 Reconstruction Algorithm

The MGPSR measurements are processed using the NASA GSFC Orbit Determination Toolbox (ODTBX) to reconstruct transmit antenna patterns for all observed GPS spacecraft. ODTBX is an open source, MATLAB based, orbit determination analysis tool primarily used for early phase mission analysis. ODTBX was developed at NASA Goddard Space Flight Center (GSFC) and includes a MATLAB version of the NAIF Spice Toolkit (called MICE). The toolbox is designed for flexibility, rapid analysis, and ease of use while maintaining the level of fidelity needed for early mission design. The Java Astrodynamics Toolbox (JAT) is used as an engine for processes that might be slow in MATLAB such as high fidelity trajectory propagation and celestial body ephemeris look-ups (via MICE). The primary analysis functions are batch least-squares and sequential filter commands with Monte-Carlo simulation, linear covariance analysis, measurement processing, and data visualization capabilities. Many measurement models and their supporting tools are available such as GPS and Deep Space Network (DSN) measurement types [18].

In addition to the GPS pseudorange measurement model, ODTBX includes a suite of GPS data analysis functions. This tool set provides the ability to model physical parameters of the transmitters and receiver (relative geometry and antenna patterns), perform link budget analyses to estimate either transmit or received power, and a full suite of plotting and visualization routines. This functionality was utilized in reconstructing the GPS transmit antenna patterns using the MGPSR data.

The pattern reconstruction process consists of two components: a core algorithm that uses the ODTBX GPS tools to reconstruct transmit gain from MGPSR receiver measurements, and an automation framework that reconstructs a full pattern from a long-term batch of measurements. Figure 6 shows a high-level overview of the process, described in detail below.

The pattern reconstruction process operates on C/N_0 measurements logged by the MGPSR receiver, resolves the receive/transmit geometry at each epoch, and performs a link budget calculation to derive the GPS-transmitted gain. The MGPSR measurements are logged daily at 30-sec intervals for each visible satellite. The reconstruction algorithm operates on each measurement for a single PRN on a single day, appending transmit azimuth and elevation angles along with calculated transmit gain.

Because the receiver measurements are associated with the GPS pseudorandom noise (PRN) spreading codes and not the GPS satellite vehicle number (SVN), PRN to SVN mapping is done using a compiled history of PRN assignments,

Table 1: GPS SVN/block mapping. Bold font indicates Block IIR satellites with the modernized antenna panel.

Block	**Tracked SVNs**
IIA	23, 26, 33–35, 38–40
IIR	41, 43–46, 51, 54, 56
IIR-M	**47**, 48, 50, 52, 53, 55, 57, 58, **59–61**
IIF	62–68

then the SVN is mapped to the vehicle block ID. All antenna pattern analysis is done by vehicle block or by individual SVN since each block of GPS satellites have a different transmit antenna design. The current constellation consists of the Boeing Block IIA and IIF vehicles and the Lockheed Martin Block IIR and IIR-M – with the "M" designation indicating the modernized payload which has a new antenna design. However, some of the later Block IIR satellites were also launched with these new antenna panels. Table 1 shows the SVN to block mapping used in this analysis, where the IIR satellites with the modernized antenna are included in the IIR-M block category and indicated as such in bold.

To calculate GPS transmit angles, the ephemeris and attitude information for both the receiving and transmitting spacecraft are needed. For the receiving vehicle, the position and velocity information is available at 60-sec intervals, and the vehicle attitude ephemeris is provided at 5-minute intervals. After performing the appropriate conversions from Earth-fixed to the Earth-centered inertial frame (J2000) and from Euler angles to attitude quaternions, the ephemerides are interpolated to the measurement times using Hermite and spherical linear interpolation, respectively.

For the GPS transmitters, the vehicle ephemerides are computed from the GPS Almanac at the epoch of the data. A model of the GPS vehicle attitude is also needed to calculate the azimuth and elevation angles for the signal originating from the transmitter. The nominal attitude of the GPS satellites points the boresight of the GPS antenna at the center of the Earth and yaws about this axis in order to keep the solar panels perpendicular to the direction of the sun. The nominal yaw angle is the angle of rotation about the +z body fixed axis (nadir) from the velocity direction of the vehicle to the +x body fixed axis that ensures the +x axis of the vehicle is pointing towards the sun. This yaw model applies to the Boeing Block IIA and IIF satellites. The nominal yaw for the Lockheed Martin Block IIR and IIR-M satellites is oriented differently with the -x axis pointed towards the sun. Figure 7 shows this geometry for the yaw angle calculation for the various satellite blocks. The GPS satellites do not follow this nominal attitude behavior during a period of eclipse (Midnight turn) or when the nominal yaw rate would be too high at orbit noon (Noon turn). Because the behavior of the GPS satellites is not well defined during these periods, Noon and Midnight turn data are not included in the antenna pattern reconstruction process. The yaw model algorithm described in [19] was implemented in MATLAB. With this information at hand, the transmit and receive azimuth and elevation angles at every epoch are computed.

With knowledge of the received power R_p, the receiver antenna gain A_r, space-loss attenuation A_d, and the transmit power of the GPS satellite P_{sv}, the gain at the transmit antenna A_t can be found. It should be noted that the link budget values shown in Table 2 for transmit power and receiver losses are preliminary and based on calibrating the link budget to match the ground measured patterns for the Block IIR and IIR-M satellites. The measured received power is a function of the noise temperature of the receiver T_s, the carrier to noise density ratio C/N_0 expressed in dBW, and contributions from other losses in the receiver N_f as shown in Equation 8.

$$R_p = (C/N_0 - 228.6) + 10log_{10}(T_s) - N_f \tag{8}$$

The space-loss in dB is a function of the distance between the transmitter and receiver r (km) and the link frequency $L1$ (Hz). Equation 9 shows the link budget equation used to find the transmitter gain.

$$A_t = R_p - A_r - A_d - P_{sv} \tag{9}$$

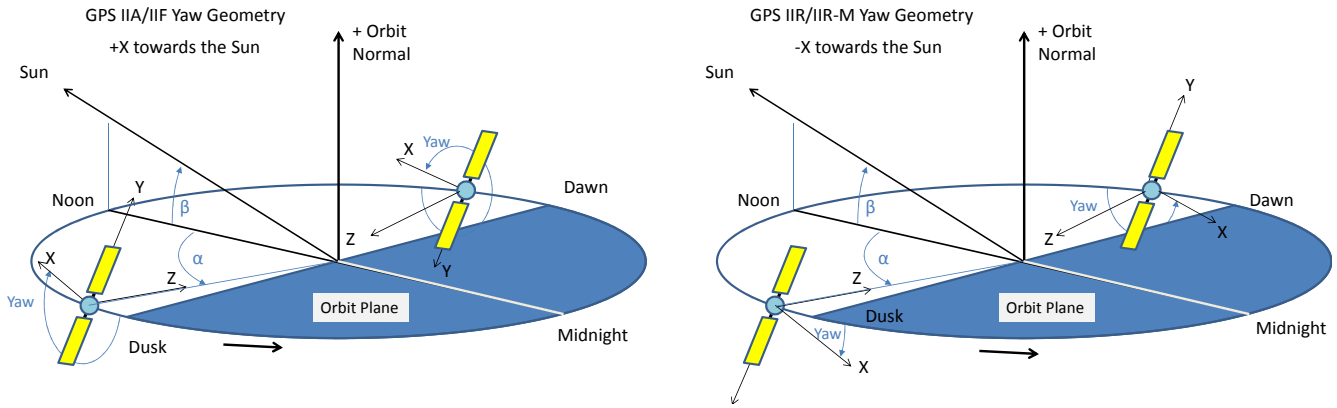

Figure 7: Geometry of the GPS transmitter yaw model for Block IIA and IIF (left) and Block IIR and IIR-M (right). The yaw angle is defined as the rotation about the nadir pointed +z body fixed axis from the velocity vector direction in the orbital plane to the +x body fixed axis.

Link Parameter	Symbol	Value	Units
Receiver Losses	N_f	-4.1	dB
Noise Temperature	T_s	290	K
Block IIA TX Power	P_{sv}	14.5	dBW
Block IIR TX Power	P_{sv}	14.6	dBW
Block IIR-M TX Power	P_{sv}	13.9	dBW
Block IIF TX Power	P_{sv}	13.9	dBW

Table 2: Constant link budget parameters assumed in the antenna gain pattern reconstruction.

The core post-processing algorithm operates on a single day of measurements for a single PRN. To generate results across a range of dates and PRNs, a batch-processing system was utilized to automate the transmit gain calculations. The computed transmit antenna gains are written to an intermediate file in 1 degree bins of transmitted azimuth and elevation angles for each SVN, one file for every day of data collection. Given a range of dates and PRNs of interest, all available data is processed and finally compiled batched results are sorted by SVN and block.

5.2 Results

The results presented in this paper focus on the transmit gain patterns reconstructed from a ten-month period and averaged over all SVNs in each block. Long-term averaging into block patterns allows for significant overlapping coverage to beyond 90 deg off-boresight and over the full 360 deg in azimuth. While that same time period is sufficient to generate full azimuthal coverage of each individual GPS vehicle, the resulting patterns appear very similar to the block averages at the resolution of the plots presented. Per-SVN transmit gain patterns will be published in a future paper.

The first set of plots compare the GPS ACE reconstructed gain patterns for Blocks IIR and IIR-M with near-field ground measurements recently made public by Lockheed Martin (LM) [9]. Figure 8 shows the LM ground data on the left and GPS ACE flight data on the right for Block IIR; Figure 9 shows the same comparison for Block IIR-M. Note that these results have IIR and IIR-M vehicles grouped by *type of antenna panel*, where the IIRs with modernized panels are grouped with the IIR-Ms (see Table 1). The plots show transmit gain on a color scale in the range of -30 to +15 dB as a function of off-boresight angle from 0 deg (center of plot) to 90 deg (outer edge) and azimuth from 0 deg (to the right) to 360 deg with positive rotation in the counter-clockwise direction. As oriented on the vehicle, the spacecraft body +x axis is to the right, the +y body axis is toward the top of the page, and the +z body axis (boresight) is out of the page. In other words, the azimuth is measured from spacecraft body +x axis positive toward spacecraft body +y for a positive rotation around body +z or the boresight direction. The center of

the GPS ACE plots has no data because the GPS signals are blocked by the earth from the vantage point in GEO.

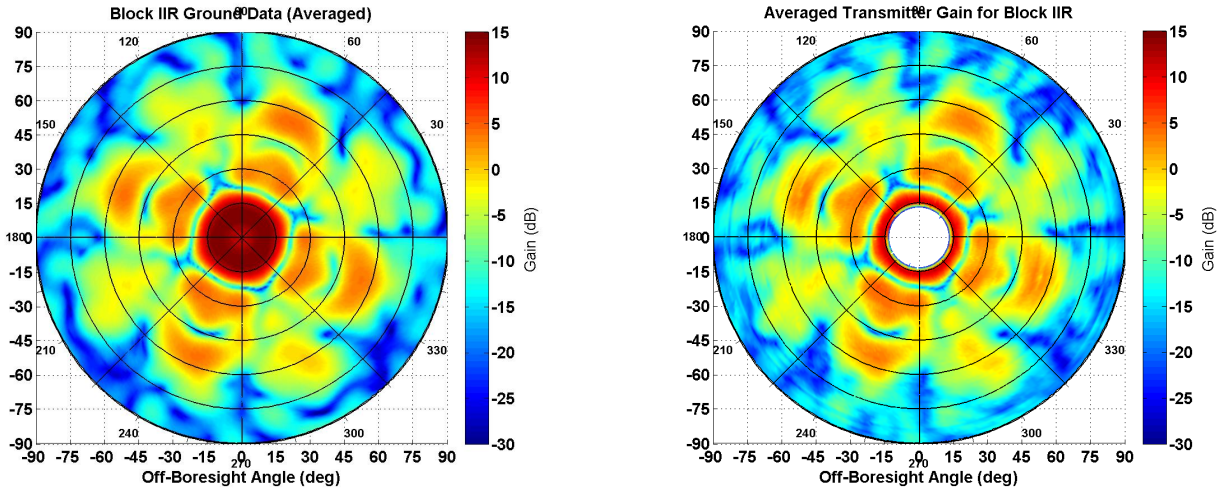

Figure 8: Comparison of **Block IIR** ground measured antenna pattern (left) to reconstructed antenna pattern from GPS ACE flight data (right). GPS ACE data was collected from all Block IIR SVs over a 10 month period and averaged in 1 deg x 1 deg bins.

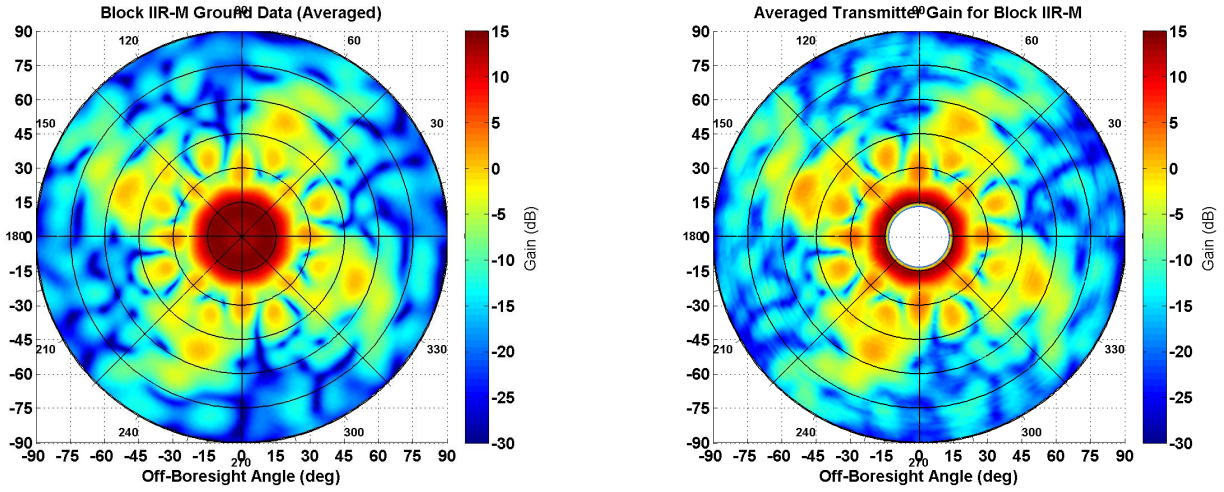

Figure 9: Comparison of **Block IIR-M** ground measured antenna pattern (left) to reconstructed antenna pattern from GPS ACE flight data (right). GPS ACE data was collected from all Block IIR-M SVs over a 10 month period and averaged in 1 deg x 1 deg bins.

Both GPS ACE results show remarkable similarity to the LM ground measurements, most clearly in the patterns of the nulls around the outer edge. For example, in Figure 8 at 180 deg azimuth on the left side of each plot, there is a distinctive feature in the null (the "claw") that does not appear anywhere else. Resolution to this level of detail can be used to verify the orientation of the panels on the spacecraft. In fact, this comparison has illuminated a discrepancy with the coordinate frame claimed by LM for its data files in Ref. [9]: 0 deg azimuth along the spacecraft body -y axis and positive rotation toward the body -x axis. However, the ground data plots in Figures 8 and 9 are plotted assuming they are aligned with the GPS ACE frame (0 deg azimuth along +x, positive toward +y), and they clearly match. If the data in the LM files were aligned with 0 deg azimuth along -y with an opposite sense of rotation, then the data would need to be rotated into the GPS ACE frame for the respective plots to match, but no such rotation has been applied. The source of this discrepancy has yet to be determined. Regardless, this comparison demonstrates that extensive ground measurements provide accurate representations of the gain patterns that appear to hold up both after installation on the spacecraft and over extensive time on orbit.

Another feature of note is the azimuthal dependence of the gain outside the main beam, including the gross four-fold symmetry and the -22.5 deg offset of the peaks of the first and second side lobes from the x and y axes. The variability of gain in azimuth highlights the shortcomings of plotting gain averaged over azimuth, particularly as off-boresight angle increases to where receivers would be tracking closer to their thresholds. It also illustrates the disadvantage of performing ground measurements at coarse azimuth cuts like every 90 deg or 45 deg and assuming uniform or average behavior in the side lobes. Full patterns such as those determined by GPS ACE provide an advantage to GPS side lobe users who could employ them for more efficient search and tracking algorithms.

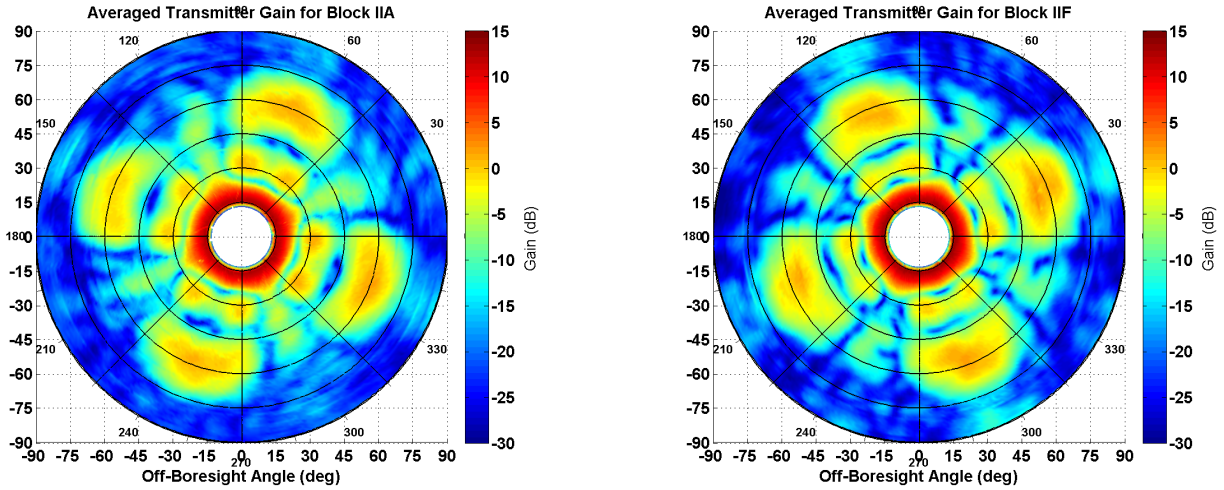

Figure 10: **Block IIA** (left) and **Block IIF** (right) antenna pattern reconstructed from GPS ACE flight data. GPS ACE data was collected from all Block IIA and IIF SVs over a 10 month period and averaged in 1 deg x 1 deg bins.

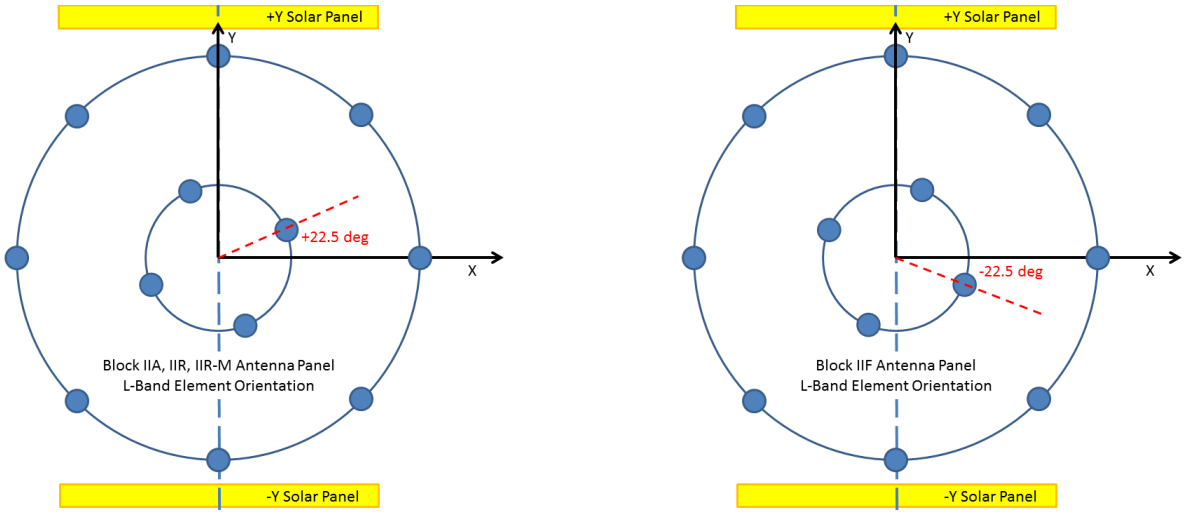

Figure 11: L-Band antenna inner and outer element orientations with respect to spacecraft body axes. The left plot depicts the orientations for **Block IIA** [20] and **Blocks IIR** and **IIR-M** [9]. The right plot depicts **Block IIF** [21]. Note the difference in the orientation of the inner elements of Block IIF.

Unlike Lockheed Martin, Rockwell/Boeing did not perform extensive ground tests of the full transmit pattern for Block IIA [3] and IIF vehicles. To be fair, there was no requirement to do so, and Boeing did take coarse measurements of the IIFs that have yet to be released publicly. The fact remains, however, that there are no references for comparison for full gain patterns of IIA and IIF vehicles. In that context, Figure 10 shows the first full representations of the IIA (left) and IIF (right) transmit gain patterns, as measured by GPS ACE. These plots are in the same orientation as the IIR and IIR-M plots such that the spacecraft body +x axis is to the right and the body +y axis is toward the top of

the page. The most obvious distinction is that, although the patterns are very similar to each other, the IIF pattern has its high side lobes clocked at +22.5 deg off the x and y axes versus -22.5 deg as in the other three blocks. This may be explained by the difference in orientation of the L-Band elements in the respective antenna arrays, shown in Figure 11. These graphics depict only the number and relative orientation of the individual L-band elements, purposefully ignoring differences in size and element construction to highlight the relative orientations. As shown in the graphic on the right, the Block IIF inner elements are oriented differently than the other blocks [20, 9, 21]. The high side lobe azimuths in Figure 10 appear to occur halfway between the azimuths of the inner elements for the respective orientations shown in Figure 11.

This is a key result for high altitude users of GPS as completion of the IIF launches nears, at which point they will comprise nearly half the GPS constellation. Without any other source of detailed side lobe data for the IIF vehicles, high altitude users who rely on side lobe observations would likely assume a pattern from an earlier block to represent the IIFs; however, the plots show that the high side lobes are 45 deg offset, which would lead to modeling errors in the link budgets for much of the GPS constellation. It is the goal of Aerospace and NASA Goddard as part of the IR&D effort to publish detailed patterns resulting from GPS ACE in order to provide this benefit to the GPS community.

6 Uses of GPS ACE Data

The transmit gain patterns for the current blocks of satellites can be used throughout the different phases of the life cycles of near-term missions. The patterns can be used in GPS signal simulators to accurately model the signal in space for space users at all altitudes. This enables not only verification of navigation requirements during the development phase of a mission, but also provides confidence on the signal availability in order to employ more stringent navigation requirements in high altitude regimes. An example is the GOES-R mission [22] which used a preliminary GPS ACE determination of the Block IIF gain to improve its modeling of the future constellation and ensure that it still met requirements. Once in operations, missions like GOES-R can use the gain patterns in satellite search/selection algorithms to more efficiently target those GPS vehicles transmitting through the higher side lobe regions of the gain patterns.

Looking farther into the future, a GPS signal measuring capability like GPS ACE can continually monitor the SSV performance of current GPS vehicles as well as newly-launched vehicles. This would be especially useful as Block III and later satellites become operational with increasing numbers of space users relying on side lobe signals. Gain patterns for each new satellite could be determined, and side lobe performance requirements could be verified against in-flight measurements.

A sample metric for SSV analysis is the average received power at GEO. Figure 12 shows preliminary estimates of the received power in dBW averaged over azimuth versus GPS off-boresight angle for the L1 C/A signals received by each block over a ten-month period. Included in the plot legend is the estimated mean power over the off-boresight angle range of 30-60 deg, with Block IIR being the obvious standout. Requirements based on this or similar metrics for future blocks which define a minimum level of performance in the side lobes would provide consistency in the expectations of signal availability for long-lived, high-altitude missions that span multiple generations of GPS vehicles.

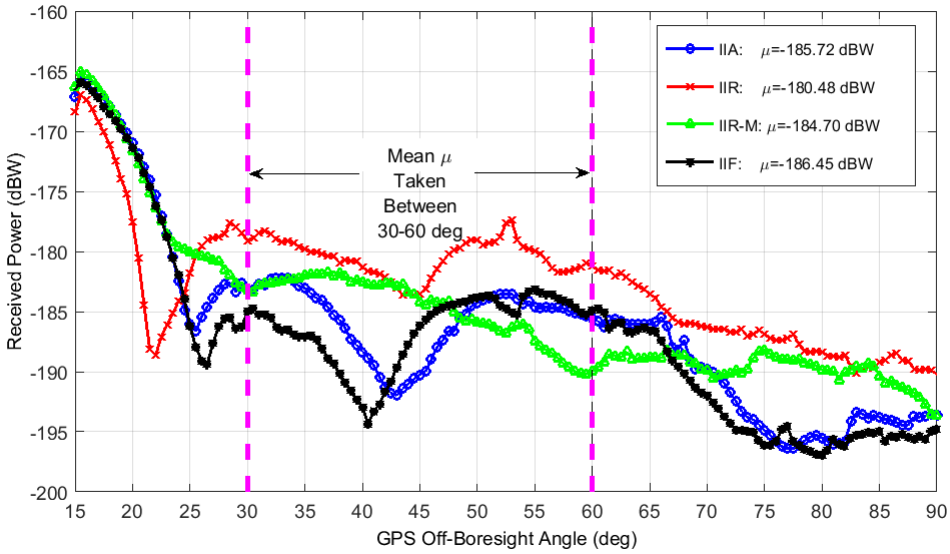

Figure 12: Preliminary estimates of *average* received power at GEO for GPS L1 C/A signal as measured by GPS ACE. These average values encompass a large absolute range as evidenced by the azimuthal variations indicated in Figures 8-10, but are conducive to side lobe performance metric definition.

7 Conclusion & Future Work

This paper demonstrates that the GPS ACE project generates abundant, high quality measurements of the GPS L1 signal in space out to beyond 90 deg off-boresight from the GPS transmit antennas. The key to the high resolution data is the unique Aerospace Mariposa GPS Receiver with sensitivity to below 0 dB-Hz, providing all-in-view tracking from GEO. Resulting average gain patterns for Blocks IIR and IIR-M are shown to agree very well with ground measurements, and results presented for Blocks IIA and IIF are the first extensive measurements produced of their complete patterns. Uses of GPS ACE data include SSV monitoring, accurate side lobe link budget simulations, satellite selection algorithm augmentation, and verification of high-altitude mission navigation requirements.

Note, however, that the analyses described in this paper relied on only one of the GPS observation types: received carrier to noise ratio. Future work will delve into characterization of the pseudorange and carrier phase measurements, including determination of pseudorange deviation maps and the effect of carrier phase smoothing. Given the long duration of data collection, another avenue of investigation will be the variability of the measurement types over time, potentially involving seasonal or Sun beta angle correlations. Finally, many of these analyses will be duplicated with the observations from the NASA Navigator receiver to evaluate consistency where it overlaps in sensitivity with the MGPSR. In addition, the unique capabilities of the Navigator receiver will be assessed, such as accuracy of its real-time point solutions and extended Kalman filter state estimates.

8 Acknowledgment

This work was performed under a collaborative Independent Research and Development effort between The Aerospace Corporation and NASA Goddard Space Flight Center authorized under Space Act Agreement SAA5-14-2-N16999.

References

[1] James D. Kronman. Experience Using GPS For Orbit Determination of a Geosynchronous Satellite. In *Proceedings of the International Technical Meeting of the ION Satellite Division*. ION GNSS, 2000.

[2] Michael C. Moreau. *GPS Receiver Architecture for Autonomous Navigation in High Earth Orbits.* PhD thesis, University of Colorado, 2001.

[3] Francis M. Czopek and Lt. Scott Shollenberger. Description and Performance of the GPS Block I and II L-Band Antenna and Link Budget. In *Proceedings of the International Technical Meeting of the ION Satellite Division.* ION GPS, September 1993.

[4] Thomas D. Powell, Philip D. Martzen, Steven B. Sedlacek, Chia-Chun Chao, Randy Silva, and Alison Brown. GPS Signals in a Geosynchronous Transfer Orbit: Falcon Gold Data Processing. In *Proceedings of the National Technical Meeting of the ION Satellite Division.* ION GNSS, January 1999.

[5] Oliver Balbach, Bernd Eissfeller, Günter W. Hein, T. Zink, Werner Enderle, Michael Schmidhuber, and Norbert Lemke. Tracking GPS Above GPS Satellite Altitude: Results of the GPS Experiment on the HEO Mission Equator-S. In *Proceedings of the 11th International Technical Meeting of the ION Satellite Division.* ION GPS, September 1998.

[6] M. C. Moreau, E. P. Davis, J. R. Carpenter, D. Kelbel, G. W. Davis, and P. Axelrad. Results from the GPS Flight Experiment on the High Earth Orbit AMSAT OSCAR-40 Spaceraft. In *Proceedings of the International Technical Meeting of the ION Satellite Division.* ION GPS, September 2002.

[7] Frank Bauer, Michael C. Moreau, M.E. Dahle-Melsaether, W.P. Petrofski, B.J. Stanton, S. Thomason, G.A. Harris, R.P. Sena, and L. Parker Temple III. The GPS Space Service Volume. In *Proceedings of the International Technical Meeting of the ION Satellite Division.* ION GPS, September 2006.

[8] Martin Unwin, Steeve Kowaltschek, Reynolt de vos Van Steenwijk, Paul Blunt, and Yoshi Hashida. Navigating Above the GPS Constellation: Preliminary Results from the SGR-GEO on GIOVE-A. In *Proceedings of the 26th International Technical Meeting of the ION Satellite Division.* ION GNSS+, September 2013.

[9] Willard Marquis and Daniel Reigh. The GPS Block IIR and IIR-M Broadcast L-Band Antenna Panel – Its Pattern and Performance. *Navigation*, Pre-publication.

[10] Luke M. Winternitz, William A. Bamford, and Gregory W. Heckler. A GPS Receiver for High-Altitude Satellite Navigation. *IEEE Journal of Selected Topics in Signal Processing*, 3(4), August 2009.

[11] Nicholas A. DiOrio and Penina Axelrad. GPS Weak Signal Detection for Orbit Determination at Geosynchronous Altitudes. Discovery Learning Student Project Poster at CU-Boulder, April 2012.

[12] B. Hofmann-Wellenhof, H. Lichtenegger, and J Collins. *GPS Theory and Practice.* Springer-Verlag Wein, third edition, 1994.

[13] Mark L. Psiaki. Block Acquisition of Weak GPS Signals in a Software Receiver. In *Proceedings of the Internation Technical Meeting of the ION Satellite Division.* ION GNSS, September 2001.

[14] J. B. Y. Tsui. *Fundamentals of Global Positioning Systems Receivers, A Software Approach.* J. Wiley and Sons, New York, 2000.

[15] John David Jackson. *Classical Electrodynamics.* John Wiley and Sons, Inc., 1962.

[16] Seymour Stein. Algorithms for Ambiguity Function Processing. *IEEE Transactions on Acoustics, Speech, and Signal Processing*, ASSP-29(3), June 1981.

[17] Willard D. Downs, III. Trace Trajectory Analysis and Orbit Determination Program, Vol. I, General Program Objectives, Description and Summary. Technical Report TR-0059(9320)-1, The Aerospace Corporation, 1971.

[18] NASA Goddard Space Flight Center. Orbit Determination Toolbox (ODTBX)^{Beta}. sourceforge.net/projects/odtbx/, 2015.

[19] Y. E. Bar-Sever. A New Model for Yaw Attitude of Global Positioning System Satellites. *The Telecommunications and Data Acquisition Progress Report 42-123*, November 1995. Available at http://tda.jpl.nasa.gov/progress_report.

[20] Christopher J. Hegarty and Eric Chatre. Evolution of the Global Navigation Satellite System (GNSS). In *Proceedings of the IEEE*, volume 96. IEEE, December 2008.

[21] Boeing. Photograph of IIF Satellite and L-Band Antenna Panel during Assembly. Available at http://www.boeing.com/space/global-positioning-system under Flexible Capabilities.

[22] Jim Chapel, Devin Stancliffe, Tim Bevacqua, Stephen Winkler, Brian Clapp, Tim Rood, David Gaylor, Doug Freesland, and Alexander Krimchansky. Guidance, Navigation, and Control Performance for the GOES-R Spacecraft. GNC 2014: 9th International ESA Conference on Guidance, Navigation & Control Systems, June 2014.